

1 **Observed impacts of COVID-19 on urban CO₂**
2 **emissions**

3 **Alexander J. Turner^{1,2,3*}, Jinsol Kim¹, Helen Fitzmaurice¹, Catherine**
4 **Newman², Kevin Worthington², Katherine Chan², Paul J. Wooldridge²,**
5 **Philipp Köhler⁴, Christian Frankenberg^{3,4}, and Ronald C. Cohen^{1,2}**

6 ¹Department of Earth and Planetary Sciences, University of California, Berkeley, CA, 94720, USA

7 ²College of Chemistry, University of California, Berkeley, CA, 94720, USA

8 ³Jet Propulsion Laboratory, California Institute of Technology, Pasadena, CA, 91109, USA

9 ⁴Division of Geological and Planetary Sciences, California Institute of Technology,

10 **Key Points:**

- 11 • Observe a 28% decrease in urban CO₂ emissions from the San Francisco Bay Area
12 in response to COVID-19 mobility restrictions
13 • Changes are primarily driven by a decrease in CO₂ emissions from traffic (-44%)
14 • Large change to the weekly and diurnal cycle of emissions with reductions in morn-
15 ing rush-hour emissions

*now at: Department of Atmospheric Sciences, University of Washington, Seattle, WA, 98195, USA

Corresponding author: Ronald C. Cohen, rccohen@berkeley.edu

Corresponding author: Alexander J. Turner, turneraj@uw.edu

Abstract

Governments restricted mobility and effectively shuttered much of the global economy in response to the COVID-19 pandemic. Six San Francisco Bay Area counties were the first region in the United States to issue a “shelter-in-place” order asking non-essential workers to stay home. Here we use CO₂ observations from 35 Berkeley Environment, Air-quality and CO₂ Network (BEACO₂N) nodes and an atmospheric transport model to quantify changes in urban CO₂ emissions due to the order. We infer hourly emissions at 900-m spatial resolution for 6 weeks before and 6 weeks during the order. We observe a 28% decrease in anthropogenic CO₂ emissions during the order and show this decrease is primarily due to changes in traffic (-44%) with pronounced changes to daily and weekly cycles; non-traffic emissions show small changes (-8%). These findings provide a glimpse into a future with reduced CO₂ emissions through electrification of vehicles.

Plain Language Summary

This work uses atmospheric observations to quantify the changes in urban CO₂ emissions from different sectors in response to COVID-19 mobility regulations.

1 Introduction

Carbon dioxide (CO₂) is an atmospheric trace gas responsible for most of the growth in anthropogenic radiative forcing (IPCC, 2013). Mitigating long-term climate change necessitates drastic reductions to our CO₂ emissions. Specifically, limiting global mean warming to 1.5°C requires reaching net-zero anthropogenic CO₂ emissions by 2050 (IPCC, 2018). Over 70% of these anthropogenic CO₂ emissions in the United States are attributable to urban areas (EIA, 2015; Hutyra et al., 2014); as such, it is important to be able to accurately quantify the emissions from these regions to support regulatory policies aimed at CO₂ reduction and provide citizens with metrics indicating their effectiveness.

The abrupt shuttering of the global economy in response to the COVID-19 global pandemic presents an opportunity to evaluate methods for quantifying urban CO₂ emissions, to assess our ability to attribute emissions to specific source sectors, and to describe the changes in emissions from different sectors. Understanding the changes that occurred during the COVID-19 period will allow us to identify: 1) the magnitude and subset of CO₂ emissions that respond to changes in our travel to/from workplaces on short time scales and 2) the sectors whose emissions persist irrespective of changes in urban travel patterns. Recent research used changes in activity data to predict the impact of COVID-19 on global CO₂ emissions and inferred a -17% (-11% to -25%) change in global daily CO₂ emissions (Le Quéré et al., 2020). This prediction has yet to be confirmed with measurements of atmospheric CO₂.

The focus of this study is the San Francisco Bay Area in Northern California as it was the first region in the United States to enact regulations on mobility through a “shelter-in-place” (SIP) order on March 16, 2020 (Contra Costa County Health Officer, 2020). We use a dense network of CO₂ observations across the north eastern region of the San Francisco Bay Area to quantify the impacts of the SIP order on urban CO₂ emissions. Figure 1A shows the spatial coverage of our ground-based network of *in situ* sensors: the Berkeley Environmental Air-quality & CO₂ Network (BEACO₂N; Shusterman et al., 2016; Turner et al., 2016; Kim et al., 2018; Shusterman et al., 2018). We examine data from the study period between February 2, 2020 and May 2, 2020, during which 35 sensors were operational.

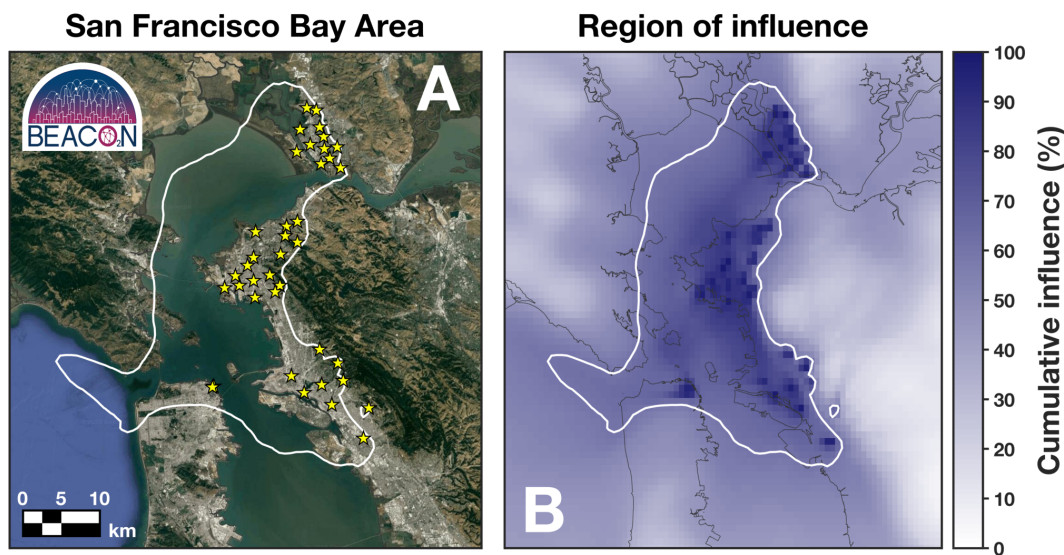


Figure 1. Observational network in the San Francisco Bay Area. Panel A shows the location of instruments in the Berkeley Environmental Air-quality & CO₂ Network (BEACO₂N; yellow stars). Panel B shows the cumulative influence to the network derived from STILT footprints for observations in March 2020. White contour in both panels indicates the region that contains the largest 40% of the total network influence (referred to as the “BEACO₂N Domain”).

61

2 Atmospheric Inversion Framework

62

63

64

65

66

67

68

69

70

71

Figure 2 shows a comparison of the network-wide CO₂ concentrations averaged for each day-of-week for six weeks before and during the SIP order. We observe a 5-50 ppm decrease in mid-week CO₂ concentrations with the most pronounced changes on Monday through Thursday during the morning rush-hour (~07:00 local time). Weekend concentrations show small differences in the median between the two time periods, although the variability is somewhat larger before the SIP. These observations suggest: 1) large reductions in CO₂ emissions occurred due to the SIP order and 2) marked changes to both the daily and weekly cycle of emissions due to shifts in human activity. Quantifying and attributing changes in CO₂ concentrations to emissions requires accounting for the coupling of meteorology and emissions.

72

73

74

75

76

77

78

79

80

81

82

83

84

85

We use the Stochastic Time-Inverted Lagrangian Transport model (STILT; Lin et al., 2003; Fasoli et al., 2018) with meteorology from the NOAA High Resolution Rapid Refresh (HRRR; Kenyon et al., 2016) to both estimate the sensitivity of each measurement to upwind emission sources and estimate the concentration upwind of our domain. Each measurement (y_i) has a unique surface sensitivity (\mathbf{h}_i) and background concentration (b_i). The measurements are related to the surface CO₂ emissions (\mathbf{x}) as: $y_i = \mathbf{h}_i \mathbf{x} + b_i$ and we use Bayesian inference to obtain hourly CO₂ emissions at 900-m spatial resolution from the atmospheric measurements. Prior fluxes are adapted from previous work (Turner et al., 2016; McDonald et al., 2014) but now use a biosphere derived from measurements of solar-induced chlorophyll fluorescence (SIF; Turner et al., 2020). Additionally, we manually inspected the 20 largest point sources to ensure they were spatially allocated to plausible locations. Errors are assumed to be Gaussian and include off-diagonal terms in both error covariance matrices. Following Rodgers (1990), we solve for the hourly posterior fluxes at 900-m spatial resolution as:

$$\hat{\mathbf{x}} = \mathbf{x}_a + (\mathbf{H}\mathbf{B})^T (\mathbf{H}\mathbf{B}\mathbf{H}^T + \mathbf{R})^{-1} (\mathbf{y} - \mathbf{H}\mathbf{x}_a) \quad (1)$$

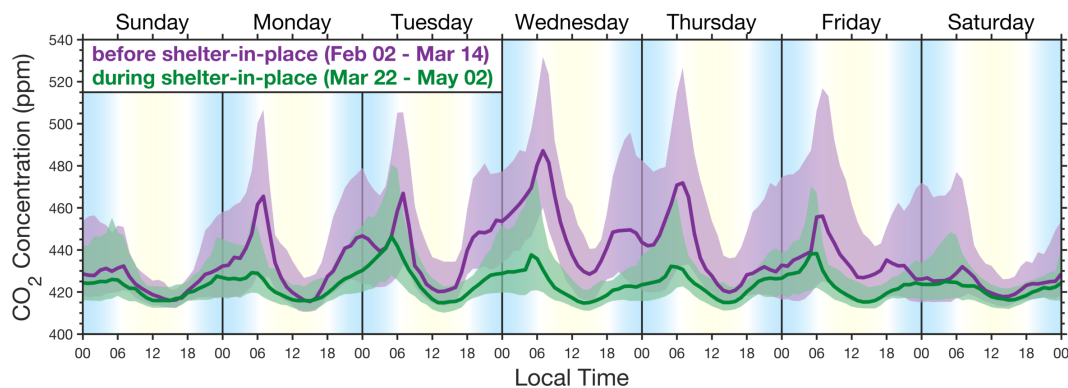


Figure 2. Weekly CO₂ concentrations before and during shelter-in-place order.

Solid lines show the median across the BEACO₂N network and the shaded region indicates the 16th to 84th percentile. Purple shows 6 weeks of data before shelter-in-place (February 2, 2020 through March 14, 2020) and green is 6 weeks during shelter-in-place (March 22, 2020 through May 2, 2020). Blue/yellow background shading is based on cosine of the solar zenith angle with white indicating dawn and dusk.

86 where $\hat{\mathbf{x}}$ ($m \times 1$) is the posterior fluxes, \mathbf{x}_a ($m \times 1$) is the prior emissions, \mathbf{y} ($n \times 1$) is
 87 the BEACO₂N observations, \mathbf{H} ($n \times m$) is the matrix of footprints from HRRR-STILT,
 88 \mathbf{R} ($n \times n$) is the model-data mismatch error covariance matrix, and \mathbf{B} ($m \times m$) is the
 89 prior error covariance matrix (see Supplemental Section S4 for additional details).

90 Posterior fluxes will reflect the prior fluxes in regions with low sensitivity from the
 91 measurements. This can be clearly seen by looking at the gain matrix $\mathbf{G} = (\mathbf{HB})^T (\mathbf{HBH}^T + \mathbf{R})^{-1}$
 92 and Eq. 1. We can see that $\hat{\mathbf{x}} \rightarrow \mathbf{x}_a$ in Eq. 1 as $\mathbf{G} \rightarrow \mathbf{0}$, indicating that our posterior
 93 solution will not deviate from the prior in regions of low sensitivity. As such, we focus
 94 our study on regions with high sensitivity because those are the regions that our obser-
 95 vations can robustly constrain. Figure 1B shows the region of influence for the BEACO₂N
 96 network. We find the network to be most sensitive to the eastern portion of the San Fran-
 97 cisco Bay Area with upwind influence extending east across the bay to San Francisco.
 98 The white contour in Figure 1B encapsulates the top 40% of the total of the network sensi-
 99 tivity, hereafter referred to as the “BEACO₂N Domain”, where we expect strong con-
 100 straints from the measurements.

101 3 High Resolution Posterior Fluxes

102 The resulting posterior fluxes inferred using BEACO₂N observations are shown in
 103 Figure 3. Figs. 3A and 3B show the spatial patterns before and during the shelter-in-
 104 place order, respectively, while Fig. 3C shows the difference. Changes on roadways are
 105 evident in the pattern of differences. Changes to other sectors are more subtle. We have
 106 high confidence in the fluxes within the BEACO₂N Domain because this is the region
 107 the BEACO₂N network is strongly sensitive to, fluxes outside of this region will revert
 108 to the prior emissions. Two spatial features that immediately stand out in Fig. 3C are:
 109 a 0.4 tC km⁻² hr⁻¹ decrease in emissions over urban areas within the BEACO₂N Do-
 110 main and a modest decrease (0.15 tC km⁻² hr⁻¹) across most of the San Francisco Bay
 111 Area. We are able to attribute these observed changes to particular sectors because of
 112 the: 1) high spatial resolution obtained here, 2) satellite observations to constrain the
 113 biosphere, and 3) detailed prior information available in the region. We find that the mod-
 114 est regional decrease is due to the biosphere and the large changes in urban areas are
 115 predominantly due to decreases in traffic.

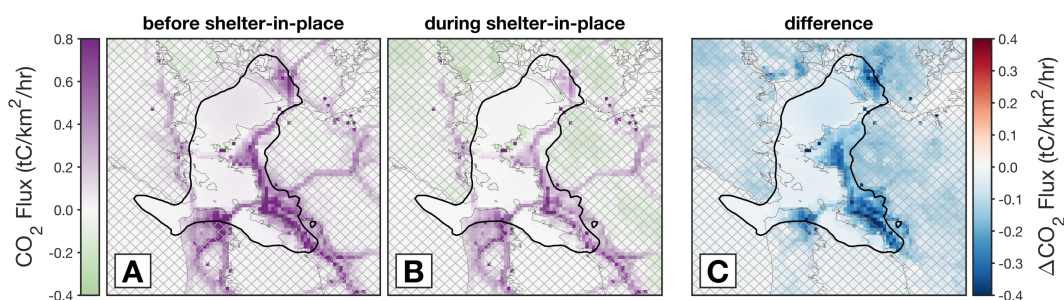


Figure 3. Spatial patterns of CO₂ fluxes in the San Francisco Bay Area. Panel A shows the average CO₂ fluxes for 6-weeks before shelter-in-place (February 2, 2020 through March 14, 2020). Panel B shows the average over 6-weeks during shelter-in-place (March 22, 2020 through May 2, 2020). Panel C is the difference. Black contour in all panels is the 60th percentile of total network influence (BEACO₂N Domain). Cross hatching indicates regions with low sensitivity to the BEACO₂N nodes.

116 Estimating CO₂ fluxes from observations during spring is complicated by the onset
 117 of photosynthesis which results in a decrease in atmospheric concentrations. In North-
 118 ern California, this begins with the grasslands and chaparral in land surrounding the ur-
 119 ban core. As mentioned above, we use high-resolution satellite observations of SIF to con-
 120 strain the biospheric activity during this time of year (see Turner et al., 2020), which have
 121 been shown to correlate strongly with photosynthetic activity (e.g., Frankenberg et al.,
 122 2011; Yang et al., 2015, and others). These space-borne SIF measurements indicate a
 123 252% (26 tC/hr) increase in daytime CO₂ uptake from the biosphere across the BEACO₂N
 124 Domain when comparing before and during the SIP order. This increase in biospheric
 125 activity inferred from space-borne SIF measurements drives the regional decrease in CO₂
 126 fluxes shown in Figure 3C.

127 The large changes within the BEACO₂N Domain coincide with major freeways in
 128 the San Francisco Bay Area. In particular, the largest decreases are observed over In-
 129 terstate 880 (I-880) that runs north-south from San Jose to Oakland. Our observational
 130 network is only sensitive to the northern half of I-880, but the entirety of that section
 131 shows decreases in CO₂ fluxes in excess of 0.4 tC km⁻² hr⁻¹. I-880 is a crucial freeway
 132 for workers commuting to San Francisco. Other freeways that serve commuters also show
 133 large decreases in CO₂ fluxes (e.g., Interstates 80 and 580).

134 We leverage the high spatial resolution obtained here to partition our posterior CO₂
 135 fluxes to specific sectors because sources spatially separate as the resolution increases.
 136 For example, McDonald et al. (2014) demonstrated that 1-kilometer spatial resolution
 137 was necessary to distinguish freeways from arterial roads. Here, we classify grid cells that
 138 have the majority of prior emissions coming from a single sector (e.g., we classify a grid
 139 cell as “traffic” if more than 50% of the prior emissions come from the traffic sector). See
 140 Supplemental Section S5 for more details.

141 Figure 4 attributes the posterior CO₂ emissions within the BEACO₂N Domain to
 142 three sectors, 1) vehicle traffic, 2) industrial point sources, home heating, and other non-
 143 vehicle related anthropogenic emissions, and 3) biogenic. On weekdays before the SIP
 144 order, vehicles are the largest source of CO₂ during daytime, while on pre-SIP weekends
 145 “other anthropogenic” are the largest daytime source. After the SIP order, “other an-
 146 thropogenic” is always the largest source. We observe the highest CO₂ emissions dur-
 147 ing the morning rush hour in the middle of the week. This peak is only present during
 148 the weekdays. Daily average emissions increase from Sunday to their maximum on Wednes-

149 day and then decrease from Wednesday to Saturday. In contrast, daily average emissions
 150 during SIP have more subtle differences between weekdays and weekends, as suggested
 151 by the day of week variation in the concentrations of CO₂ shown in Figure 2. Weekday
 152 emissions start earlier than on weekends before and after the SIP order. After the SIP,
 153 rush hour emissions are lower but they still extend emissions earlier and later than seen
 154 on weekends, resulting in a flatter weekday daytime emissions profile than on weekends.
 155 Emissions from vehicles at night pre-SIP averaged ~150 tC/hr and during SIP the night-
 156 time emissions averaged ~60 tC/hr. This represents a 61% decrease in nighttime emis-
 157 sions and a 39% decrease during daytime (245 to 157 tC/hr).

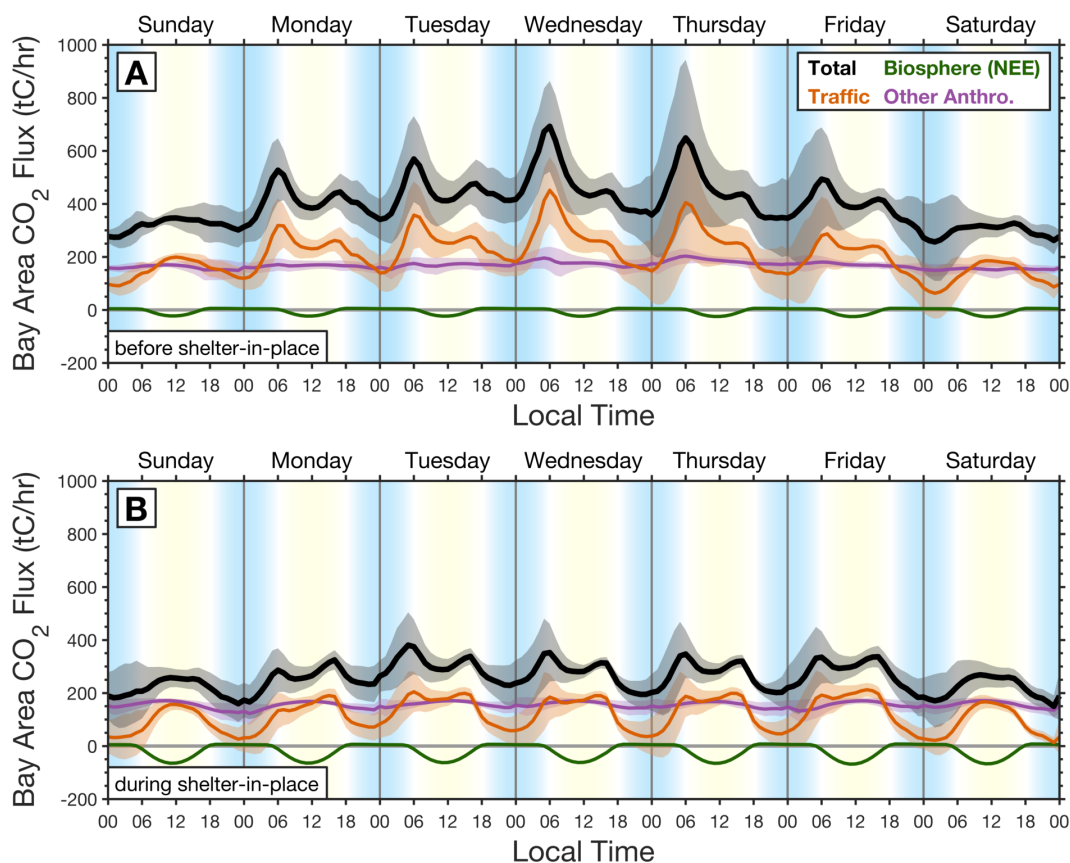


Figure 4. Weekly cycle of CO₂ fluxes before and during shelter-in-place order.

Solid lines are the weekly mean CO₂ fluxes over the BEACO₂N Domain (40th percentile shown in Fig. 1) and shading is 1- σ . Black are the total fluxes. Orange are the traffic emissions. Purple are other anthropogenic emissions: industrial point sources, residential heating, and other non-vehicle anthropogenic sources. Green are the biosphere fluxes (Net Ecosystem Exchange; NEE). Panel A shows emissions before shelter-in-place (February 2, 2020 through March 14, 2020) and panel B shows emissions during shelter-in-place (March 22, 2020 through May 2, 2020).

158 We find a -44% change (-91 tC/hr) in the weekly average CO₂ emissions from grid
 159 cells that are classified as freeway whereas emissions from non-traffic anthropogenic sources
 160 (“Other Anthro.” in Figure 4) only decreased by 8% (-13 tC/hr). Much of this decrease
 161 in non-traffic anthropogenic sources occurs at night. Independent data from the Cali-
 162 fornia Department of Transportation also indicates a 41% and 34% decrease in vehicle
 163 miles traveled by cars and trucks, respectively, for road segments in the BEACO₂N Do-
 164 main (Caltrans, 2020). The posterior emissions indicate a small diurnal cycle in this sec-

165 tor that is largely absent before the SIP order and is not present in the prior emissions.
 166 Such sectoral changes are possible to observe here due to the densely spaced nodes in
 167 the BEACO₂N network, allowing us to obtain sub-kilometer spatial resolution and re-
 168 solve different sectors.

169 4 Conclusions

170 This unnatural experiment conducted in response to COVID-19 has demonstrated
 171 the subset of CO₂ emissions that are elastic and those that are more entrenched. Emis-
 172 sions from traffic are highly elastic and could be rapidly mitigated in response to either
 173 technological advances or regulations. In contrast, the non-traffic emissions (e.g., indus-
 174 trial sources and residential heating) showed minimal changes in response to the shelter-
 175 in-place order. This implies that those sources are more entrenched and will require longer-
 176 time scales to mitigate if we hope to limit future warming. These findings provide a glimpse
 177 into a future where CO₂ emissions from vehicle traffic are reduced through the electri-
 178 fication of the vehicle fleet, which would also have air quality co-benefits; observing these
 179 CO₂ emission changes from such a transition will require sustained measurements as the
 180 changes will be more subtle than the abrupt 45% changes seen here.

181 Acknowledgments

182 We thank B. Fasoli for recent developments to the STILT model and sharing pre-processing
 183 code, P. Vannucci and A. Lall for feedback, and former members of the BEACO₂N project
 184 for establishing the network: A. A. Shusterman, V. Teige, and K. Lieschke. We thank
 185 the participants of the Keck Institute for Space Studies workshop on COVID-19 and Earth
 186 System Science for feedback. We are grateful to the team that has realized the TROPOMI
 187 instrument, consisting of the partnership between Airbus Defence and Space, KNMI, SRON,
 188 and TNO, commissioned by NSO and ESA. **Funding:** AJT was supported as a Miller
 189 Fellow with the Miller Institute for Basic Research in Science at UC Berkeley. This re-
 190 search was funded by grants from the Koret Foundation and University of California,
 191 Berkeley. This research used the Savio computational cluster resource provided by the
 192 Berkeley Research Computing program at the University of California, Berkeley (sup-
 193 ported by the UC Berkeley Chancellor, Vice Chancellor for Research, and Chief Infor-
 194 mation Officer). **Author contributions:** AJT and RCC wrote the text with feedback
 195 from all authors. JK, HF, CN, KW, KC, and PJW collected CO₂ data. PK and CF per-
 196 formed the TROPOMI SIF retrieval. AJT conducted the numerical modeling, analysis,
 197 downscaled SIF data, and drafted figures. **Competing interests:** The authors declare
 198 no competing interests. **Data and materials availability:** CO₂ is available at <http://beacon.berkeley.edu/>.
 199 Code has been deposited in GitHub, https://www.github.com/alexjturner/BEACON_XXXX.

200 References

- 201 Caltrans. (2020). *Performance Measurement System Data Source*. California Depart-
 202 ment of Transportation. Retrieved from <http://pems.dot.ca.gov>
- 203 Contra Costa County Health Officer. (2020). *Contra Costa County Shelter-in-
 204 Place Order*. Contra Costa County. Retrieved from [https://cchealth.org/
 205 coronavirus/pdf/H0-COVID19-SIP-0316-2020.pdf](https://cchealth.org/coronavirus/pdf/H0-COVID19-SIP-0316-2020.pdf)
- 206 EIA. (2015). *Emissions of Greenhouse Gases in the U.S.* (Tech. Rep.). U.S. Energy
 207 Information Administration.
- 208 Fasoli, B., Lin, J. C., Bowling, D. R., Mitchell, L., & Mendoza, D. (2018). Sim-
 209 ulating atmospheric tracer concentrations for spatially distributed receptors:
 210 updates to the Stochastic Time-Inverted Lagrangian Transport model's R
 211 interface (STILT-R version 2). *Geoscientific Model Development*, 11(7), 2813-
 212 2824. doi: 10.5194/gmd-11-2813-2018
- 213 Frankenberg, C., Fisher, J. B., Worden, J., Badgley, G., Saatchi, S. S., Lee, J.-E.,

- 214 ... Yokota, T. (2011). New global observations of the terrestrial carbon cycle
 215 from GOSAT: Patterns of plant fluorescence with gross primary productivity.
 216 *Geophys Res Lett*, *38*(17). doi: 10.1029/2011gl048738
- 217 Hutyra, L. R., Duren, R., Gurney, K. R., Grimm, N., Kort, E. A., Larson, E., &
 218 Shrestha, G. (2014). Urbanization and the carbon cycle: Current capabilities
 219 and research outlook from the natural sciences perspective. *Earth's Future*,
 220 *2*(10), 473-495. doi: 10.1002/2014ef000255
- 221 IPCC. (2013). *Climate Change 2013: The Physical Science Basis. Contribution*
 222 *of Working Group I to the Fifth Assessment Report of the Intergovernmental*
 223 *Panel on Climate Change* (Tech. Rep.). Author.
- 224 IPCC. (2018). *Global Warming of 1.5°C. An IPCC Special Report on the im-*
 225 *pacts of global warming of 1.5°C above pre-industrial levels and related global*
 226 *greenhouse gas emission pathways, in the context of strengthening the global*
 227 *response to the threat of climate change, sustainable development, and efforts*
 228 *to eradicate poverty* (Tech. Rep.). Author.
- 229 Kenyon, J. S., Moninger, W. R., Smith, T. L., Peckham, S. E., Lin, H., Grell, G. A.,
 230 ... Manikin, G. S. (2016). A North American Hourly Assimilation and Model
 231 Forecast Cycle: The Rapid Refresh. *Monthly Weather Review*, *144*(4), 1669-
 232 1694. doi: 10.1175/mwr-d-15-0242.1
- 233 Kim, J., Shusterman, A. A., Lieschke, K. J., Newman, C., & Cohen, R. C. (2018).
 234 The BERkeley Atmospheric CO₂ Observation Network: field calibration and
 235 evaluation of low-cost air quality sensors. *Atmospheric Measurement Tech-*
 236 *niques*, *11*(4), 1937-1946. doi: 10.5194/amt-11-1937-2018
- 237 Le Quéré, C., Jackson, R. B., Jones, M. W., Smith, A. J. P., Abernethy, S., Andrew,
 238 R. M., ... Peters, G. P. (2020). Temporary reduction in daily global CO₂
 239 emissions during the COVID-19 forced confinement. *Nature Climate Change*.
 240 doi: 10.1038/s41558-020-0797-x
- 241 Lin, J. C., Gerbig, C., Wofsy, S. C., Andrews, A. E., Daube, B. C., Davis, K. J., &
 242 Grainger, C. A. (2003). A near-field tool for simulating the upstream influ-
 243 ence of atmospheric observations: The Stochastic Time-Inverted Lagrangian
 244 Transport (STILT) model. *J Geophys Res-Atmos*, *108*(D16), 4493-4510. doi:
 245 Artn4493Doi10.1029/2002jd003161
- 246 McDonald, B. C., McBride, Z. C., Martin, E. W., & Harley, R. A. (2014). High-
 247 resolution mapping of motor vehicle carbon dioxide emissions. *J Geophys Res-*
 248 *Atmos*, *119*(9), 5283-5298. doi: Doi10.1002/2013jd021219
- 249 Rodgers, C. D. (1990). Characterization and Error Analysis of Profiles Retrieved
 250 from Remote Sounding Measurements. *J Geophys Res-Atmos*, *95*(D5), 5587-
 251 5595. doi: Doi10.1029/Jd095id05p05587
- 252 Shusterman, A. A., Kim, J., Lieschke, K. J., Newman, C., Wooldridge, P. J., &
 253 Cohen, R. C. (2018). Observing local CO₂ sources using low-cost, near-
 254 surface urban monitors. *Atmos Chem Phys*, *18*(18), 13773-13785. doi:
 255 10.5194/acp-18-13773-2018
- 256 Shusterman, A. A., Teige, V. E., Turner, A. J., Newman, C., Kim, J., & Co-
 257 hen, R. C. (2016). The BERkeley Atmospheric CO₂ Observation Net-
 258 work: initial evaluation. *Atmos Chem Phys*, *16*(21), 13449-13463. doi:
 259 10.5194/acp-16-13449-2016
- 260 Turner, A. J., Köhler, P., Magney, T. S., Frankenberg, C., Fung, I., & Cohen,
 261 R. C. (2020). A double peak in the seasonality of California's photo-
 262 synthesis as observed from space. *Biogeosciences*, *17*(2), 405-422. doi:
 263 10.5194/bg-17-405-2020
- 264 Turner, A. J., Shusterman, A. A., McDonald, B. C., Teige, V., Harley, R. A., &
 265 Cohen, R. C. (2016). Network design for quantifying urban CO₂ emissions:
 266 assessing trade-offs between precision and network density. *Atmos Chem Phys*,
 267 *16*(21), 13465-13475. doi: 10.5194/acp-16-13465-2016
- 268 Yang, X., Tang, J., Mustard, J. F., Lee, J.-E., Rossini, M., Joiner, J., ... Richard-

269 son, A. D. (2015). Solar-induced chlorophyll fluorescence that correlates
270 with canopy photosynthesis on diurnal and seasonal scales in a temper-
271 ate deciduous forest. *Geophysical Research Letters*, 42(8), 2977-2987. doi:
272 10.1002/2015gl063201